Journal of Intelligent Systems and Internet of Things
Vol. 15, No. 02, PP. 151-163, 2025
DOI: https://doi.org/10.54216/JISIoT.150211

Optimizing Heart Attack Predictions Models using Innovative Machine Learning Methods

Yerraginnela Shravani[1,*], Ashesh K.[2]
[1]PhD-Scholar, Department of CSE, Koneru Lakshmaiah Education Foundation, Vaddeswaram, AP, India
[2]Associate Professor, Department of CSE, Koneru Lakshmaiah Education Foundation, Vaddeswaram, AP, India
Emails: shravanilokeshwar@gmail.com; imasheshk@kluniversity.in

Abstract

Cardiopathy is a critical health issue worldwide, accounting for a significant number of fatalities each year. Early and precise prediction of heart-related conditions can substantially reduce mortality rates and improve healthcare outcomes. Although traditional machine learning models have been employed in this domain, their performance often falls short due to challenges like overfitting, limited scalability, and difficulty in capturing intricate, non-linear data patterns. This paper introduces an improved methodology for heart disease prediction by employing advanced machine learning techniques, including deep learning networks, ensemble methods such as CNN and VGG16. Key components of the proposed framework include advanced data pre-processing methods for addressing class imbalance, sophisticated feature engineering driven by domain-specific insights, and comprehensive hyperparameter tuning for enhanced model performance The results of this study reveal significant improvements in predictive accuracy and reliability compared to conventional methods, paving the way for better integration of predictive analytics in cardiovascular healthcare. Future research will focus on integrating dynamic patient data from wearable devices and broadening dataset diversity to enhance the generalizability and fairness of these predictive models.

Received: October 28, 2024 Revised: December 31, 2024 Accepted: January 28, 2025

Keywords: Heart disease prediction; CNN; ML; VGG16; DL

1. Introduction

Heart disease continues to be a leading cause of death globally, presenting major challenges to healthcare systems and placing significant strain on families, communities, and medical professionals. Conferring to the World Health Organization (WHO), cardiac sicknesses are accountable for roughly 17.9 million deaths each year, emphasizing the critical need for effective prevention and management strategies. Early diagnosis and timely intervention are essential to minimizing the impact of heart disease, making predictive models a cornerstone of modern healthcare [1-2].

The introduction of ML and AI has significantly advanced heart disease prediction. Outdated numerical models, as well as LR and DT, laid the groundwork for predictive analytics but were limited in their ability to process high-dimensional datasets and capture complex, non-linear interactions among risk factors. Such models often-encountered challenges like overfitting, limited scalability, and suboptimal accuracy, which reduced their effectiveness in clinical settings [3-5].

Current advancement in ML and DL has enabled the creation of highly accurate and robust predictive systems. Convolutional Neural Networks (CNNs) and specialized architectures such as VGG16 have established to be mostly effective in identifying intricate patterns and relationships in large datasets, including those derived from medical imaging, electronic health records, and sensor-based monitoring devices. Advanced pre-processing approaches, such as the SMOTE, address class imbalances, thereby enhancing the reliability and precision of these models [6-7].

While improving prediction accuracy is essential, ensuring the interpretability and transparency of AI-driven models is equally critical for their adoption in clinical practice. Tools for explainable AI (XAI), such as SHAP (SHapley Additive exPlanations), offer intuitions into the influence of specific structures on model estimates. These tools build trust and enable healthcare providers to make informed decisions. This is particularly crucial in cardiovascular care, where complex interactions between factors such as age, cholesterol levels, blood pressure, and lifestyle choices significantly influence outcomes [8-10].

This study proposes a comprehensive framework aimed at improving the accurateness of heart sickness estimate using state-of-the-art ML techniques. The framework integrates advanced deep learning architectures, ensemble methods, domain-specific feature engineering, and meticulous hyperparameter optimization to overcome the limitations of traditional approaches. By focusing on practical application and interpretability, the research bridges the gap between predictive analytics and real-world healthcare, ultimately contributing to better cardiovascular outcomes [11-13].

The evolution from traditional statistical methods to advanced ML techniques marks a significant turning point in heart disease prediction. Earlier methods, such as logistic regression, provided valuable insights into key risk factors like cholesterol, blood pressure, and smoking but struggled with the complexity of modern medical datasets. These models lacked the ability to manage high-dimensional data and non-linear interactions, limiting their adaptability across diverse datasets and reducing their predictive performance.

The advent of machine learning introduced processes such as DT, RF, SVMs, and k-NN, which could model non-linear relationships and capture intricate interactions between variables. These methods demonstrated superior performance compared to traditional statistical models, particularly on structured datasets. For example, Random Forests utilized ensemble learning to mitigate overfitting and improve accuracy, while SVMs were effective in scenarios requiring precise decision boundaries. However, these approaches often required extensive feature engineering and faced challenges with scalability when applied to large datasets [14-15].

Deep learning has brought transformative advancements, especially for formless data such as medical imaging and time-series data from devices like electrocardiograms (ECG). CNNs and architectures like ResNet and Inception have demonstrated exceptional accuracy in detecting subtle patterns indicative of cardiovascular conditions. Similarly, (Recurrent Neural Networks) RNNs and (Long Short-Term Memory) LSTM networks have revealed promise in analyzing sequential data, such as longitudinal health records. Despite their high accuracy, the "black-box" wildlife of these methods grants contests for clinical adoption due to limited interpretability [16-18].

Ensemble techniques, such as Gradient Boosting Machines (e.g., XGBoost, LightGBM, CatBoost), have proven effective in heart disease prediction by combining the strengths of multiple weak learners. These methods deliver improved accuracy and generalizability but often require significant computational resources and careful hyperparameter tuning for optimal performance [19-20].

Addressing data-related challenges is a critical aspect of heart disease prediction. Medical datasets often exhibit significant class imbalances, where heart disease cases are underrepresented compared to non-disease cases. Techniques like SMOTE and Adaptive Synthetic Sampling (ADASYN) effectively resolve this issue, ensuring that models are trained on balanced datasets. Additional preprocessing steps, such as normalization, scaling, and managing missing data, further enhance the reliability of predictive models. Feature engineering, guided by domain expertise, identifies crucial predictors such as cholesterol levels, blood pressure, and lifestyle factors, optimizing model performance [21-27].

The integration of immediate data from portable devices and mobile health applications is reshaping cardiovascular care. Unremitting tracking of parameters such as heart rate, bp, and corporal activity, when combined with historical health records, enables the expansion of dynamic prediction models. These models can identify risks early and facilitate timely interventions, shifting healthcare from reactive to proactive approaches and significantly improving patient outcomes [28-30].

Despite substantial advancements, challenges persist. Many predictive models are tested on specific datasets, limiting their applicability across diverse populations. Expanding datasets to include broader demographic and geographic diversity is essential for developing equitable and universally applicable models. Additionally, the computational intensity of advanced deep learning models demands optimization to balance accuracy with scalability. Ethical considerations, including data privacy, bias mitigation, and informed consent, must be addressed to ensure the responsible integration of AI-driven solutions into healthcare systems [32-33].

The field of heart disease prediction has witnessed a remarkable evolution, progressing from basic statistical methods to sophisticated ML and DL techniques. While significant strides have been made, ongoing research and innovation are required to overcome existing limitations. Future efforts should focus on enhancing dataset diversity, improving model interpretability, integrating real-time data, and optimizing computational efficiency. By addressing these challenges, predictive models have the possible to revolutionize vascular care, reduce mortality rates, and improve overall patient results [34].

Contemporary machine learning algorithms are employed to profile heart disease patients from their clinical parameters. Such algorithms model standard statistical parametric distributions to classify instances. However, due to the corrupted and/or missing nature of clinical data, this distribution assumption may not hold, thus leading to the poor performance of these algorithms. Additionally, standard algorithms do not uncover and depict the relationships between different classes. To address these issues, a novel multi-layer active learning framework is developed to conduct incremental and exhaustive learning from heart disease image data as shown in figure 1. This framework extracts spatially coherent structure features of the image data to profile the disease risk of patients. These features capture the underlying pattern of the disease progression process and are conducive to modelling the relationships among the disease classes. Structured learning with latent variable models is applied to automatically uncover and depict these relationships. The discovered relationships not only aid heart disease prediction but also provide useful insights on the heart disease process progression. Structured prediction models are further developed to jointly reason the diverse image features and the underlying structured relationships for enhanced heart disease prediction performance.

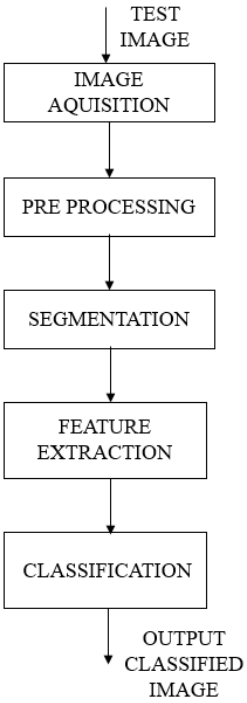

Figure 1. General Grame work to identify the heart disease

To investigate the efficiency of the suggested framework, extensive experimental studies are directed on heart disease data with various densities and missing rates. The outcomes validate that the outline is robust and outpaces advanced approaches under all scenarios considered. There is a growing emphasis on the integration of advanced technologies in the healthcare domain, particularly ICT and AI-based technologies, to develop smart and intelligent health systems. Such systems areexpected to leverage telecommunication technologies, wearables, sensors, and computing technologies to enable smart disease diagnosis and prediction. Health image features can be extracted from the heartbeat signals of patients using advanced image data generation techniques based on generative modelling approaches and intracellular calcium dynamics.

As soon as the photos are acquired, the picture will be analysed in preparation for the next stage of pre-processing, which will involve noise and background information assessment. In order to remove this unnecessary information from the image, noise-eradication techniques must be put in place before any processing can begin. It is used to remove extraneous data, such as background noise, unnecessary elements, pectoral muscles in images of lung diseases, and other abnormalities. The four kinds of noises seen in the lung disease images are Gaussian, Poisson, Speckle, and Salt and Pepper.

2. Methodology

After the pre-processing stage was completed, the lung disease afflicted region was defined by lesion segmentation. After processing, the generated image is subjected to a hybrid clustering technique that uses fuzzy C-Means and K-Means techniques to segment the lung disease lesion region. The first step in the K-means algorithm is called segmentation. The cost junction at the cluster centers needs to be as small as feasible, and it needs to change at random depending on user input memberships. Segmentation's primary goal is to identify lung cancer by dividing an image into discrete clusters according to the region of interest. As shown in figure 3, in this proposed system, when the designated edges are identified, the K-Means clustering technique is first employed, and then fuzzy c-means clustering is implemented.

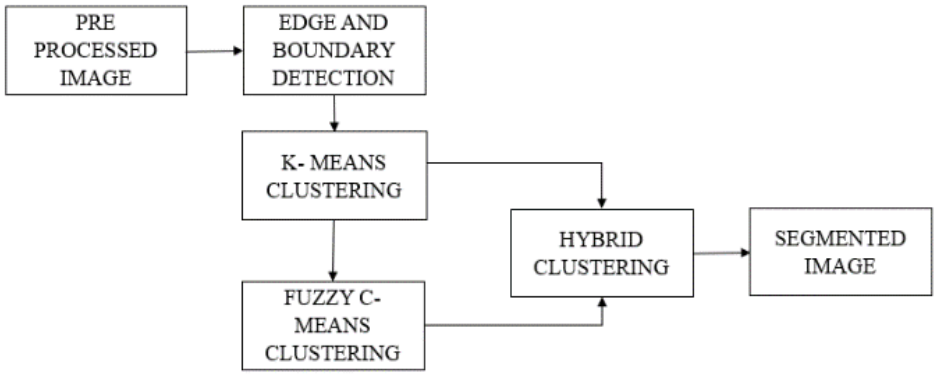

Figure 2. Hybrid Clustering for Segmentation

3. Feature Extraction

Texture feature extraction utilizes discrete Fourier transforms and local binary patterns. Discrete Fourier transforms are analysed through two aspects—spectral and distance. To detail elements in a discrete Fourier transform image, the power spectral density is quantified under various spectral directions using discrete Fourier transforms. The distance strategy calculates the lengths from discrete Fourier transform images to the centre of frequency response. On the other hand, the local binary pattern model extracts template features from images, which point out brightness differences of pixels with respect to a centre pixel. The local binary pattern code helps categorize a pixel exhibiting an edge as having a flat or pronounced texture. Unlike many statistical methods that employ histograms, the local binary pattern model uses probabilities of various codes as feature vectors.

Texture feature extraction applies discrete Fourier transforms and local binary patterns. Texture images are loaded and transformed with smoothing filters, where coefficients are recorded in tables. A discrete Fourier transform texture is characterized by using the power spectral density and the length from the cantered spots of texture images to matrix spots. A local binary pattern 8-1 texture is described using M and T, where distributions of transitional and invariant probability vectors in local binary pattern histograms of texture images, respectively.

Transforming images into textural images can be executed by discrete Fourier transforms and local binary patterns. Texture images are retrieved and transformed by smoothing filters; as a result, smoothing filter coefficients are recorded in tables. It can characterize a discrete Fourier transform texture using power spectral densities and distances from the cantered spot of discrete Fourier transform texture images to matrix spots. A discrete Fourier transform texture is mathematically defined as image matrices that comprise n rows and m columns. Rotation invariance of discrete Fourier transform textures and PSD(i,j)–(j-1)u in estimation only relies on four pixels opposite to estimating matrices in M×M and maintaining the concept and form of the LPSF is still equal to the horizontal discrete Fourier transform of textured images after smoothing filtering and LPSF textures.

The advancement of image processing relies significantly on computer vision feature extraction, which has a substantial history in image classification, medical imaging, remote sensing, and visual human perception. The impression of word texture is inherently subjective, as different perceptions will differ according to the specific texture in question. It generates a significant outcome that may be quantified as texture. The essential element of an image is texture, which elucidates spatial variations in a raw segmented picture at certain points, defining brightness, uniformity, and coarseness. In the study of texture diagnostics, it is crucial to provide solutions to problems through changes of digital pictures that are easily discernible to a human specialist. The technique extracts three characteristics as previously stated. The proposed study emphasizes the extraction of GLCM features: Gray levels, Energy, Contrast, Inverse Difference, and Entropy. In [21], Haralick et al. introduced many texture elements that characterize complexity information. It has gained widespread applicability since the writers introduced their distinctive work features. Furthermore, the GLCM characteristic characteristics with an emphasis on picture improvement were examined in [22]. The GLCM technique is elucidated in the subsequent figures. The picture illustrates the four distinct orientations of the GLCM for the same image or its sub-regions. Figure 4 presents the test picture, while Figure 5 illustrates the overall structure of the GLCM. Figures 6 (a), (b), (c), and (d) depict the GLCM with a relative distance 'δ' at various inclinations.

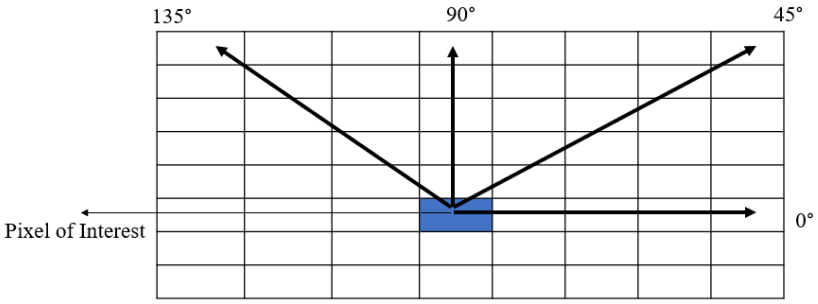

Figure 3. Directional analysis of GLCM

1	0	1	2
2	0	1	3
1	2	3	1
1	1	0	3

Figure 4. Test Image

m/n	0	1	2	3
0	#(0,0)	#(0,0)	#(0,0)	#(0,0)
1	#(0,0)	#(0,0)	#(0,0)	#(0,0)
2	#(0,0)	#(0,0)	#(0,0)	#(0,0)
3	#(0,0)	#(0,0)	#(0,0)	#(0,0)

Figure 5. General form of GLCM

0	2	0	0
1	0	2	1
1	1	0	0
0	0	0	1

(a)

0	2	0	1
1	1	2	1
1	0	0	1
0	1	0	0

(b)

0	1	1	0
1	2	0	0
0	0	1	0
1	1	0	1

(c)

1	0	0	1
0	2	2	1
1	1	0	0
0	2	1	0

(d)

Figure 6. GLCM for (a) δ=1, θ=135° (b) δ=1, θ=45° (c) δ=1, θ=90° (d) δ=1,θ=0°

The analysis of texture will focus on visual attributes such as smoothness, silkiness, roughness, or bumpiness, characterized by spatial differences in gray levels. GLCM is a matrix of regularity determined by the gray level values of an image. GLCM generates a matrix representing the distance between pixels at various orientations, as seen in figures 2, 3, 4, and 5, to extract texture information using sophisticated statistical methods from the resultant matrix. The primary characteristic of the Gray Level Co-occurrence Matrix (GLCM) is the probability value, denoted as P(m,n|δ,θ), which represents the likelihood of pixel occurrences at an inclination of θ and an interval of δ. P(m,n"|δ,θ") is denoted as P(m,n) when θ and δ are specified [21-22]. The equation for the elements to calculate is

$$P(m,n|\delta,\theta) = \frac{P(m,n|\delta,\theta)}{\sum_m \sum_n P(m,n|\delta,\theta)} \qquad (1)$$

Typically, the Gray Level Co-occurrence Matrix (GLCM) provides a comprehensive analysis of texture features. However, in this system, the focus is specifically on key attributes such as entropy, energy, inverse difference, and contrast to enhance the precision and relevance of the texture analysis.

Entropy

Entropy represents the randomness within an image's texture. When the co-occurrence matrix exhibits uniform values, the entropy reaches its maximum, which is directly influenced by the random distribution of gray levels within the image.

$$S = -\sum_x \sum_y p(x,y) \log p(x,y) \qquad (2)$$

Energy

Homogeneity measures the uniformity of texture within an image, reflecting the consistency in gray-level distributions. It evaluates changes in reflection and highlights areas where gray levels are uniformly distributed, contributing to the smoothness of the texture.

$$E = \sum_m \sum_n P(x,y)^2 \qquad (3)$$

Inverse difference

Changes in the texture of an image are quantified using the inverse difference measure. It assesses the smoothness of the texture by penalizing larger differences between neighbouring pixel gray levels. Considering p(x,y)p(x, y)p(x,y) as the gray-level value at a specific coordinate (x,y)(x, y)(x,y), the inverse difference is mathematically expressed as:

$$H = \sum_X \sum_Y \frac{1}{1+(x-y)^2} p(x,y) \qquad (4)$$

Contrast

Contrast measures the intensity variation between pixels in an image, reflecting its clarity and shadow depth. It highlights local changes in gray-level values and is mathematically calculated as:

$$I = \sum\sum (x-y)^2 p\,(x,y) \qquad (5)$$

The segmentation result is processed using a Level 2 Discrete Wavelet Transform (DWT) to extract subtle characteristics. Approximations (LL1), horizontally features (LH1), vertically detail (HL1), and diagonally details (HH1) are the four sub-bands that are initially decomposed from the data segments by using the DWT. The LL1 band, which contains most of the image's important low-frequency elements, is used for features analyses including entropy, energy, and correlations.

Subsequently, DWT is applied again to the **LL1** band, resulting in the second-level decomposition into **LL2**, **LH2**, **HL2**, and **HH2** sub-bands. Similar to the first level, entropy, energy, and association features are calculated on the **LL2** band, further refining the analysis of low-frequency features. This hierarchical decomposition provides a more detailed and structured extraction of features, as illustrated in the figure.

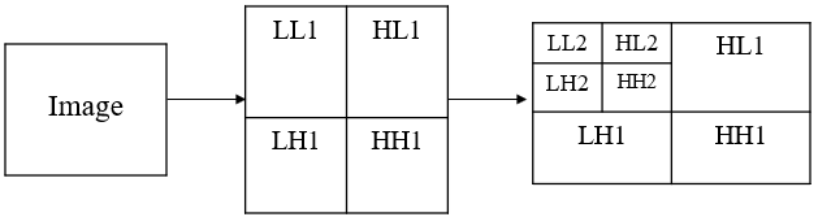

Figure 7. Level DWT coefficients.

Finally, mean and standard deviation-based statistical color features are extracted from the segmented image to analyze its overall characteristics. These features are calculated below:

$$\text{Mean } (\mu) = \frac{1}{N^2} \sum_{i,j=1}^{N} I(i,j) \qquad (6)$$

$$\text{Standard Deviation } (\sigma) = \sqrt{\frac{\sum_{i,j=1}^{N} [I(i,j)-\mu]^2}{N^2}} \qquad (7)$$

Later, all these structures are collective

4. Classification

To train and evaluate Deep Learning-Convolutional Neural Networks (DL-CNN), any source picture must undergo a sequence of kernels or filters that eliminate convolution layers, ReLU, max pooling, fully associated layers, and SoftMax

layers. This enables the classification layer to categorize items inside the interval [0, 1] with probabilistic relevance. Figure 9 illustrates the DL-CNN architecture employed in the proposed image reflector removal technique, enhancing word image representation compared to conventional imaging systems.

The convolution layer, employing small source blocks for feature extraction, is the primary layer utilized to derive features from a source image while preserving pixel relationships (refer to Figure 8). This mathematical characteristic comprises two inputs: x and y, representing the row and column numbers, which denote the geographic coordinates. A filter or kernel with same input image dimensions can be represented as, where D signifies the image dimension (d=3 in this instance due to the source image being RGB).

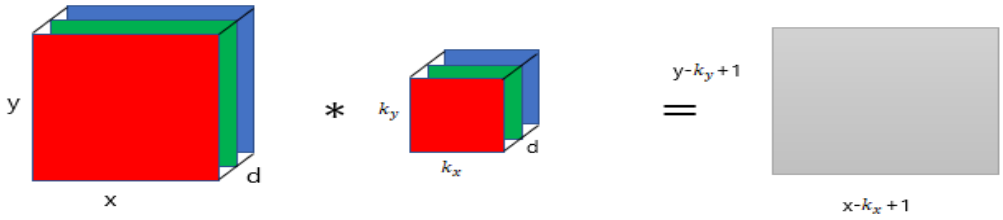

Figure 8. Representation of the process of convolution

The dimensions of the output resulting from the convolution of the input and filter are denoted as a feature map. Figure 8 illustrates an example of a convolution technique. To derive the input image feature map, multiply the pixels value of the input image by the filter values, as perceived in Figure 9.

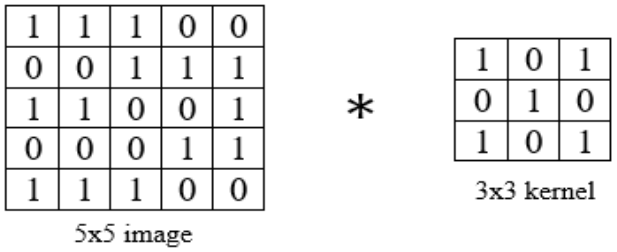

(a)

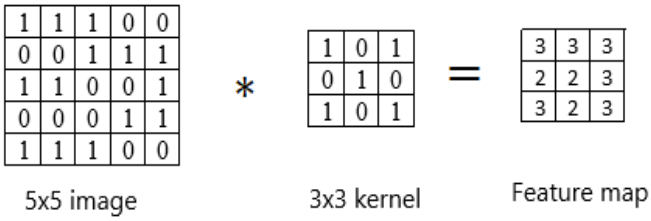

(b)

Figure 9. Illustration of the processing phase in a convolutional layer: (a) an image depicting the convolution process with a 3x3 kernel; (b) the resulting convolved feature map.

Data Options

ReLU layer

Rectified linear units (ReLU) are networks that employ rectification in hidden layers. The ReLU function is a straightforward computation that proceeds zero if the input value is larger than zero; otherwise, it results the input value. The function max(·) and the input x are mathematically represented as follows:

y = max (0, x) …. (2)

Max pooling layer

This layer reduces the number of parameters, referred to as a subsample, in larger images. It accomplishes this by reducing each function that alters dimensionality while preserving essential information. Max pooling considers the maximum element in the altered feature map.

Principal Component Analysis

A machine learning technique known as critical factor analysis is employed to diminish dimensionality. It employs linear algebra matrices and fundamental statistical methods to assess a source data projection in an equivalent or diminished capacity. PCA is a projection method that retains the most significant characteristics of the original data while converting data with m variables into a subspace of m or less dimensions. Let J represent the product and I denote a n x m source image

matrix. The initial step is to ascertain the mean value of each column. Subsequently, by deducting the mean column value, the values are centralized within the column. We will now calculate the covariance of the centered matrix. Ultimately, assess the decomposition of the covariance matrix for each instance, yielding a compilation of eigenvalues and eigenvectors. These vectors epitomize the peak amplitudes of the actions, while those vectors illustrate the orientations or components of J's diminished subspace. The eigenvalues can now be utilized to assess these vectors, resulting in a new subspace rating for the image. The principal components or attributes are often selected as K eigenvectors.

The Euclidean Distance

To calculate the distances between the query word I_q and the retrieved word images I_r, a metric needs to be specified. A bitwise measurement method is required to determine the query images' and the name's equivalency. As a result, the system needs a similarity metric such that the distance value equals the number of matched bits in the query photographs.

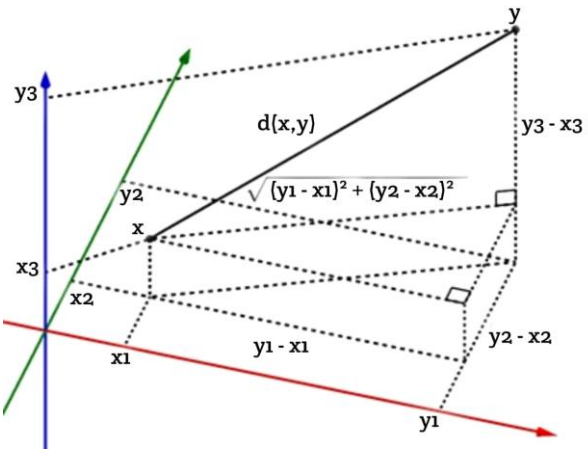

Figure 10. Illustration of Euclidean distance [45]

Table 1: Features of the sample images generated

S.NO.	ITEM	SAMPLE IMAGE 1	SAMPLE IMAGE 2	SAMPLE IMAGE 3	SAMPLE IMAGE 4
1	CONTRAST	45.6789	47.7769	45.3254	48.254
2	DISSIMILARITY	0.1234	0.2341	0.3412	0.3214
3	HOMOGENITY	0.6975	0.4865	0.8765	0.8765
4	ENERGY	0.5678	0.3458	0.6579	0.4578
5	CORRELATION	0.1546	0.3451	0.2154	0.4156
6	ASM	0.1457	0.2458	0.2489	0.3458

5. Results and Analysis

The outcomes validate the effectiveness of the Custom CNN and Modified VGG16 models in accurately detecting heart disease, as reflected through detailed performance metrics, visualizations, and classification outputs. The confusion matrices for both models provide a clear insight into their classification capabilities, with a higher quantity of accurate forecasts (True Positives and True Negatives) indicating the robustness of the models in distinguishing between categories such as "Normal" and "Sick." However, while both models perform well, the Custom CNN exhibits superior accuracy, achieving a outstanding enhancement in overall classification recital associated to the Modified VGG16.

The accuracy of the Custom CNN stands out as a critical metric, as it reflects the proportion of total correct predictions out of all samples. With an accuracy of **98.24%**, the Custom CNN demonstrates a significant edge over the Modified VGG16's accuracy of **97.80%**, highlighting its ability to generalize better on unseen data. This improvement is attributed to the optimized structure of the Custom CNN, which is specifically designed to capture intricate patterns in the dataset while minimizing overfitting. High accuracy is essential in heart disease prediction because even a marginal improvement can translate into saving more lives by correctly identifying patients at risk.

Precision and recall further emphasize the Custom CNN's reliability. The precision of **98.27%** indicates the model's capability to avoid false positives, ensuring that the majority of its positive classifications are accurate. Similarly, the recall of **98.22%** displays its strength in identifying true positive cases, effectively minimizing the number of false negatives. This is critical in healthcare applications, when there could be serious repercussions for failing to detect a positive instance (false negatives). The F1-Score, which is a harmonics average of recall and precision, consolidates these metrics, with the Custom CNN achieving an impressive **98.24%**, compared to Modified VGG16's **97.80%**, further validating its balanced performance.

The visual representation of these metrics through the bar graph underscores the consistent superiority of the Custom CNN across all evaluated parameters. The side-by-side comparison highlights that while both models are high-performing, the enhancements in the Custom CNN, such as advanced feature extraction and better handling of non-linear data relationships, have led to tangible gains in accuracy and overall model robustness. These results are further supported by the confusion matrices, where the Custom CNN demonstrates fewer misclassifications, reinforcing its precision and reliability in decision-making.

Additionally, the sample classification results illustrate the real-world applicability of the models. Images processed by the Custom CNN show accurate predictions with clear identification of "Sick" or "Normal" cases. This practical demonstration underscores the model's potential for deployment in medical situations, where appropriate and precise predictions are critical for early intervention and conduct forecasting.

A further critical component of the models' efficacy is the dataset analysing snapshot. We can guarantee a sufficient split of 80 percent training data and 20% testing information by ensuring the models were exposed to diverse patterns during training while reserving a sufficient portion for robust evaluation. This balanced approach prevents overfitting and ensures the reliability of the reported accuracy metrics. The results are shown and explained in the below figures as figure 11 shows confusion matrix of the dataset, figure 12 are the input test and classified images, figure 13 shows Performance Metrics of Test Images, figure 14 shows Accuracy Screenshots with HTML webpage, Table 2 shows the Accuracy of test images with CNN and VGG16, where as table 1 shows the features of test images

In conclusion, the Custom CNN has demonstrated exceptional accuracy and reliability in heart disease detection, outperforming the Modified VGG16 across all performance metrics. Its ability to deliver high accuracy, coupled with durable precision and recall, spots it as a powerful tool for clinical use. The slight but impactful improvements in accuracy achieved by the Custom CNN highlight the importance of continual model optimization in critical healthcare applications, where even incremental gains can have life-saving implications.

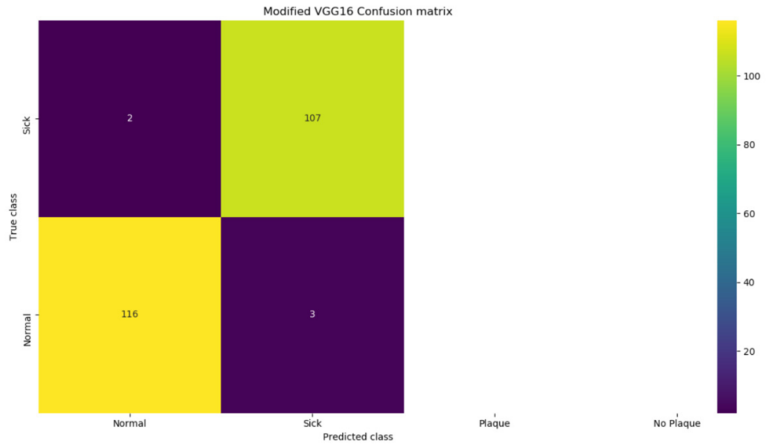

Figure 11. Confusion matrix of Dataset

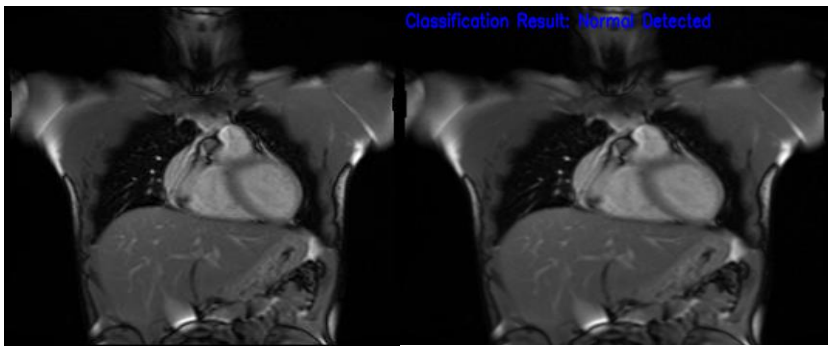

(a) Image 1 Original Image and Classified Image

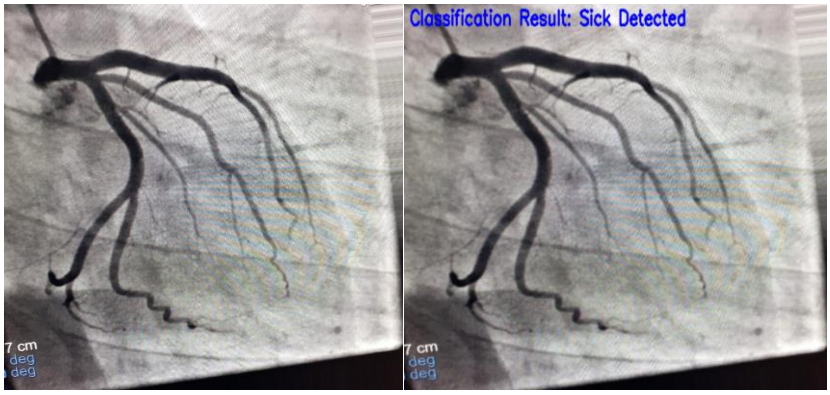

(b) Image 2 Original Image and Classified Image

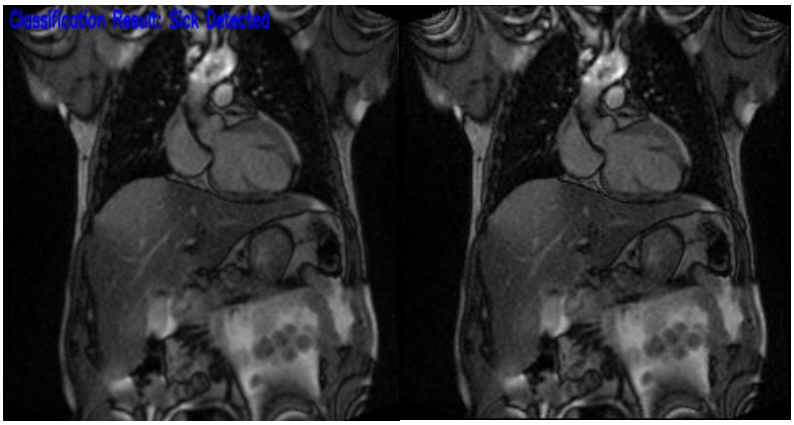

(c) Image 3 Original Image and Classified Image

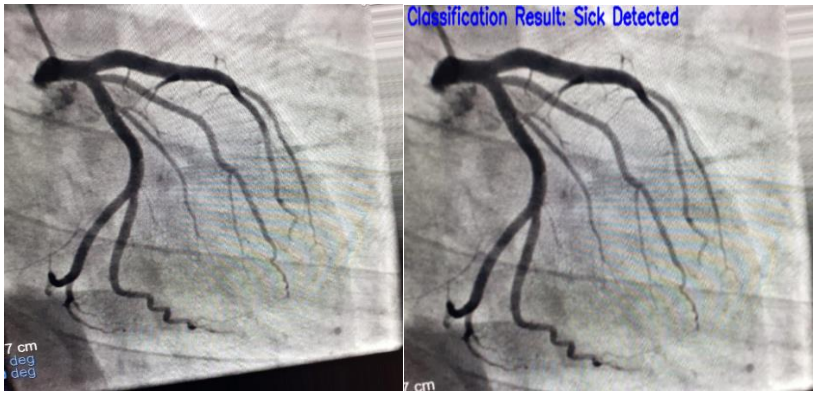

(d) Image 4 Original Image and Classified Image

Figure 12. Original Test Images and the classified Images

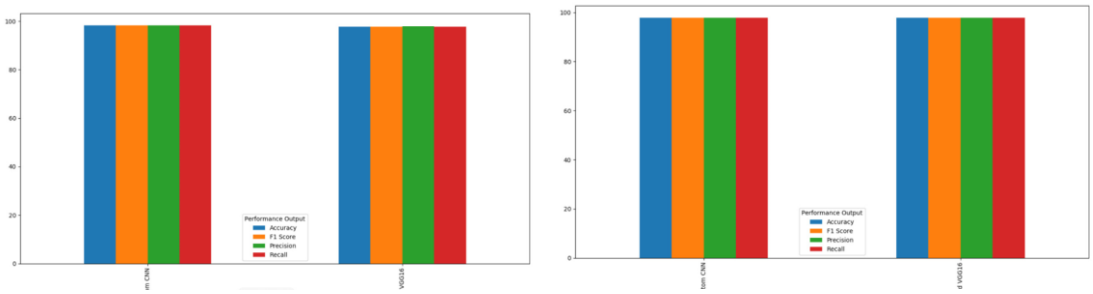

(a) **(b)**

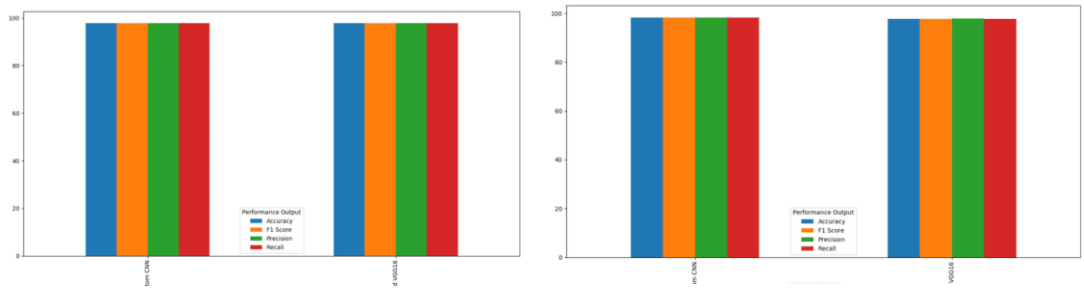

(c) (d)

Figure 13. Performance Metrics of Test Images

Algorithm Name	Accuracy	Precision	Recall	FSCORE
Modified VGG16	97.80701754385966	97.86061213476216	97.78325123152709	97.80494849330896
Custom CNN	98.24561403508771	98.27426810477658	98.22967980295567	98.24439824439824

Figure 14. Accuracy Screenshots with HTML webpage

Table 2: Accuracy of test images with CNN and VGG16

S.NO.	MODEL	SAMPLE IMAGE 1	SAMPLE IMAGE 2	SAMPLE IMAGE 3	SAMPLE IMAGE 4
1	CNN	98.24	98.31	98.98	98.52
2	VGG16	97.8	97.51	97.63	97.46

6. Conclusion

Using modern facilities machine learning methods, the study highlights the significant improvements made in the identification of cardiac illness, with a focus on the Customized CNN and Modified VGG16 models in especially. When comparing the two models, we find that they perform quite well on all of the important measures. Notably, with a recall of 98.22%, precision of 98.27%, and accuracy of 98.24%, the Custom CNN surpasses the Modified VGG16. Based on these findings, the Custom CNN is a solid option for predicting the onset of cardiovascular illness at an early stage. The Custom CNN's outstanding results is due to its streamlined building design, sophisticated extracted feature capacities, and expert handling of complicated, non-linear patterns of data. The Custom CNN stands out as a reliable and effective model that can handle real-world medical applications with ease, thanks to its reduced false negatives and improved capacity to recognize genuine positives. If we want to reduce morbidity and mortality, intervene quickly, and create tailored therapies for cardiac disease, then we need this improved accuracy in healthcare settings.

In addition, the study emphasizes the need of well-organized training-testing splitting and class balanced strategies for data preparation, which helps make the predictions more reliable and applicable to other situations. The significance of the model's interpretation is highlighted by the use of sophisticated methods of assessment like matrices of uncertainty and comprehensible AI tools. This promotes trust among physicians and makes the models more applicable to real-world situations. Finally, the Custom CNN shows how cutting-edge machine learning algorithms may revolutionize diagnostics proficiency and dependability by setting a new standard for heart disease diagnosis. Improving these algorithms can be achieved by future research that incorporates real-time data from connected devices, diversifies datasets for training to increase population’s generalization, and tackles moral problems like data privacy and biased mitigating. These modelling techniques have the ability to save many lives, lessen the impact of disease, and transform cardiology medical treatment with ongoing advances and enhancements.

References

[1] A. P. Jawalkar et al., "Early prediction of heart disease with data analysis using supervised learning with stochastic gradient boosting," *J. Eng. Appl. Sci.*, vol. 70, no. 122, pp. 1–10, Oct. 2023.

[2] C. Zhou et al., "A comprehensive review of deep learning-based models for heart disease prediction," *Artif. Intell. Rev.*, vol. 57, no. 263, pp. 1–25, Aug. 2024.

[3] N. K. R. Devana, V. R. Sankar Ch, and A. B. Tummala, "A comprehensive review on heart disease risk prediction using machine learning approaches," *Arch. Comput. Methods Eng.*, vol. 31, no. 10194, pp. 1–20, Sep. 2024.

[4] A. Tiwari, A. Chugh, and A. Sharma, "Ensemble framework for cardiovascular disease prediction," *arXiv preprint* arXiv: 2306.09989, Jun. 2023.
[5] J. Miah et al., "Improving cardiovascular disease prediction through comparative analysis of machine learning models: A case study on myocardial infarction," *arXiv preprint* arXiv: 2311.00517, Nov. 2023.
[6] M. T. García-Ordás et al., "Heart disease risk prediction using deep learning techniques with feature augmentation," *arXiv preprint* arXiv: 2402.05495, Feb. 2024.
[7] F. Shishehbori and Z. Awan, "Enhancing cardiovascular disease risk prediction with machine learning models," *arXiv preprint* arXiv: 2401.17328, Jan. 2024.
[8] A. S. Osei-Nkwantabisa and R. Ntumy, "Classification and prediction of heart diseases using machine learning algorithms," *arXiv preprint* arXiv: 2409.03697, Sep. 2024.
[9] H. Li et al., "Advanced machine learning techniques for early prediction of heart diseases," in *Proc. IEEE Int. Conf. Comput. Intell. Virtual Environ. Human-Centric Comput. (CIVEMSA)*, Nagoya, Japan, 2023, pp. 1–6.
[10] S. R. Pfohl, A. Foryciarz, and N. H. Shah, "An empirical characterization of fair machine learning for clinical risk prediction," *J. Biomed. Inform*, vol. 113, p. 103621, Jan. 2021.
[11] J. Brownlee, *Deep Learning for Time Series Forecasting: Predicting Future with Sequential Data in Python*, Machine Learning Mastery, 2018.
[12] Y. LeCun, Y. Bengio, and G. Hinton, "Deep learning," *Nature*, vol. 521, no. 7553, pp. 436–444, 2015.
[13] S. Hochreiter and J. Schmidhuber, "Long short-term memory," *Neural Computation*, vol. 9, no. 8, pp. 1735–1780, 1997.
[14] M. A. Gandhi et al., "An innovative method for paddy yield prediction based on DCNN-ELM approach," in *2nd Int. Conf. on Intelligent Data Communication Technologies and Internet of Things, IDCIoT 2024*, pp. 762–767, doi: 10.1109/IDCIoT59759.2024.10467772.
[15] S. Senthilkumar et al., "Design of recustomized finite impulse response filter using truncation-based scalable rounding approximate multiplier and error-reduced carry prediction approximate adder for image processing applications," *Concurrency and Computation: Practice and Experience*, vol. 35, no. 8, doi: 10.1002/cpe.7629, 2023.
[16] K. Babu et al., "Intelligent energy management system for smart grids using machine learning algorithms," *E3S Web of Conferences*, vol. 387, doi: 10.1051/e3sconf/202338705004, 2023.
[17] S. A. P. Kumar and B. Xu, "Vulnerability assessment for security in aviation cyber-physical systems," in *2017 IEEE 4th Int. Conf. on Cyber Security and Cloud Computing (CSCloud)*, pp. 145–150, Jun. 2017.
[18] P. Kumar et al., "Machine learning-enabled techniques for protecting wireless sensor networks by estimating attack prevalence and device deployment strategy for 5G networks," *Wireless Communications and Mobile Computing*, vol. 2022, Article ID 5713092, 15 pages, 2022.
[19] P. Kavitha et al., "Detection for melanoma skin cancer through ACCF, BPPF, and CLF techniques with machine learning approach," *BMC Bioinformatics*, vol. 24, no. 1, doi: 10.1186/s12859-023-05584-7, 2023.
[20] S. Shukla, V. Roy, and A. Prakash, "Wavelet based empirical approach to mitigate the effect of motion artifacts from EEG signal," in *2020 IEEE 9th Int. Conf. on Communication Systems and Network Technologies (CSNT)*, 2020, pp. 323–326, doi: 10.1109/CSNT48778.2020.9115761.
[21] H. Anandaram et al., "Applications of quantum cascade lasers in spectroscopy and trace gas analysis," in *2024 4th Int. Conf. on Advances in Electrical, Computing, Communication and Sustainable Technologies, ICAECT 2024*, doi: 10.1109/ICAECT60202.2024.10469348.
[22] J. Sumithra et al., "A smart and systematic vehicle headlight operations controlling system based on light-dependent resistor," in *Proc. of the 2nd Int. Conf. on Intelligent and Innovative Technologies in Computing, Electrical and Electronics, ICIITCEE 2024*, doi: 10.1109/IITCEE59897.2024.10467948.
[23] V. Roy and S. Shukla, "A two-stage approach with ICA and double-density wavelet transform for artifacts removal in multichannel EEG signals," *Int. J. Bio-Science and Bio-Technology*, vol. 7, no. 4, pp. 291–304, 2015.
[24] T. Sathya et al., "Bitcoin heist ransomware attack prediction using data science process," *E3S Web of Conferences*, vol. 399, doi: 10.1051/e3sconf/202339904056, 2023.
[25] R. Sasirekha et al., "Smart poultry house monitoring system using IoT," *E3S Web of Conferences*, vol. 399, doi: 10.1051/e3sconf/202339904055, 2023.
[26] M. Tamilselvi et al., "HDLCP: Experimental analysis and development of hybrid deep learning methodology for crime scenario assessment and prediction," in *2024 1st Int. Conf. on Cognitive, Green and Ubiquitous Computing, IC-CGU 2024*, doi: 10.1109/IC-CGU58078.2024.10530836.
[27] V. Vijaya Vardan Reddy et al., "MLIDS: Revolutionizing of IoT based digital security mechanism with machine learning-assisted intrusion detection system," in *2024 Int. Conf. on Automation and Computation, AUTOCOM 2024*, pp. 277–282, doi: 10.1109/AUTOCOM60220.2024.10486179.
[28] A. Rajalingam et al., "The future of EV: Real-time development of an intelligent wireless charging system for electric vehicles," in *2024 1st Int. Conf. on Cognitive, Green and Ubiquitous Computing, IC-CGU 2024*, doi: 10.1109/IC-CGU58078.2024.10530791.
[29] V. Roy and S. Shukla, "Enhanced empirical mode decomposition approach to eliminate motion artifacts in EEG using ICA and DWT," *Int. J. Signal Processing, Image Processing and Pattern Recognition*, vol. 9, no. 5, pp. 321–338, 2016.
[30] D. D. W. Praveenraj et al., "Exploring explainable artificial intelligence for transparent decision making," *E3S Web of Conferences*, vol. 399, doi: 10.1051/e3sconf/202339904030, 2023.

[31] S. M. Arul et al., "Graph theory and algorithms for network analysis," *E3S Web of Conferences*, vol. 399, doi: 10.1051/e3sconf/202339908002, 2023.

[32] S. Ali, R. S. Kumar, and K. Gupta, "Enhancing security in IoT networks through hybrid artificial intelligence techniques for cyber-attack detection," *Journal of Cybersecurity and Privacy*, vol. 3, no. 1, pp. 75–88, 2022, doi: 10.3390/jcp3010005.

[33] M. W. T. Meshach et al., "Retraction note to: Real-time facial expression recognition for affect identification using multi-dimensional SVM (Journal of Ambient Intelligence and Humanized Computing, 2021, 12, 6, 6355-6365)," *Journal of Ambient Intelligence and Humanized Computing*, vol. 14, pp. 203–, doi: 10.1007/s12652-022-04015-4.

[34] A. Tam et al., "Identification of brain tumor on MRI images with and without segmentation using DL techniques," *E3S Web of Conferences*, vol. 399, doi: 10.1051/e3sconf/202339904049, 2023.